Yuxuan Zhang[1], Xiaoqiang Zhai[2], Zihao Zhou[1], Xiaolin Wang[1]

Numerical Exploration of Flow and Thermal Performance in Packed-Bed Cold Storage Enhanced by Structured PCM Capsule Layouts

[1]Research School of Engineering, The Australian National University, Canberra, ACT 2601, Australia
[2]Institute of Refrigeration and Cryogenics, Shanghai Jiao Tong University, Shanghai, 200240, China

Abstract

Understanding how the layout of phase change material (PCM) capsules influences the performance of cold thermal storage systems advances designs that maximize energy storage capacity, minimize energy losses, and improve the overall sustainability of cooling applications. Based on the closest packing principle of the crystal structure, two layouts of the spheres in cylindrical packed beds, i.e. face-centered cubic (FCC) and hexagonal closest packed (HCP), are proposed in this paper. The flow and heat transfer performance of these two packing layouts is numerically investigated. Firstly, efforts are made to figure out the thermal-hydraulic mechanisms of different packing layouts under laminar steady flows. They are compared with the conventional aligned dense layer (ADL) packing with Reynolds number in the range of 1–200. The results show that, compared with the ADL packing, the theoretical PCM packing density for HCP and FCC layouts is raised by 22.5%, thus considerably saving the space required of the packed bed. FCC packing layout achieves the best flow and thermal performance, followed by HCP packing. Secondly, PCM transient thermal performance in the whole packed beds with the three packing layouts are studied during the charging process. It is found that the FCC bed has the highest heat transfer capability at a constant flow rate of 100 L/h, with a shorter charging time by 21.4% compared to that of the conventional ADL packing.

***Keywords**: phase change material; packed-bed cold storage; energy storage density; charging time; pressure loss*

Nomenclature

A	surface area (m^2)
c	specific heat capacity ($J \cdot kg^{-1} \cdot K^{-1}$)
d	diameter (m)
d_h	pore-scale hydraulic diameter (m)
D	diameter of packed unit (m)
h	sensible heat of phase change material ($kJ \cdot kg^{-1}$)
H	total enthalpy of phase change material ($kJ \cdot kg^{-1}$)
ΔH	latent heat of phase change ($kJ \cdot kg^{-1}$)
JF	overall thermal performance factor
k	thermal conductivity ($W \cdot m^{-1} \cdot K^{-1}$)
L	length (m)
n	number of data
Re	Reynolds number
Nu_{aver}	surface average Nusselt number
p	pressure (Pa)
q_s	heat flux of the active ball ($W \cdot m^{-2}$)
t	time (s)
T	temperature (ºC)
$\overline{T}_f$	volume average temperature of HTF (ºC)
$\overline{T}_s$	surface average temperature of the active ball (ºC)
T_r	temperature at the time of τ by simulation (ºC)
T_r'	temperature at the time of τ by experiment (ºC)
u	velocity ($m \cdot s^{-1}$)
V	volume (m^3)
x	distance (m)

Greek symbols

ρ	density ($kg \cdot m^{-3}$)
φ	porosity
τ	time step (s)

Subscripts

f	heat transfer fluid
i	i-th direction
in	inlet
ini	initial time
p	phase change material
s	surface of the spherical capsule

Abbreviations

ADL	aligned dense layer
BCC	body-centred cubic
FCC	face-centred cubic
HCP	hexagonal closest packed
HTF	heat transfer fluid
MAPE	Mean Absolute Percentage Error
PCM	phase change material

SC simple cubic

TES thermal energy storage

RBC red blood cell

RMSE root mean square error

1. Introduction

As environmental problems are getting increasingly severe, the utilization of renewable energy resources becomes a hot topic of common concern (Gielen et al., 2019). However, most of the renewable energy is intermittent and periodical by nature, which makes it difficult to be harnessed in real applications if there were no appropriate measures (Helm & Mier, 2019). Under this context, thermal energy storage (TES), which stores thermal energy to bridge the mismatch between energy supply and demand, is widely applied in various areas, such as solar thermal systems, waste heat recovery and air conditioning systems (Fleuchaus et al., 2018). Compared with sensible TES, latent thermal energy storage is more favorable due to its high energy storage density and isothermal behavior during the phase change process (Diao et al., 2019).

With the development of phase change materials (PCMs), a number of studies have been conducted for cold storage applications. Fin tube phase change cold storage has been widely studied with the annular fin pitch and the number and height of fins as the key structural metrics for optimization (Zhai et al., 2015). With the advancement of PCM encapsulations, packed-bed cold storage has attracted extensive interest for its high storage density and large heat transfer area (Bindra et al., 2013; Chen et al., 2019). There are four widely studied areas regarding packed-bed cold storage, of which one is the formation of cold storage units. A cascaded packed-bed PCM cold storage unit was numerically studied by Cheng et al. (Cheng & Zhai, 2018a) and compared with a single-stage cold storage unit. The results showed that a 24-stage cold storage with a phase change temperature difference between the highest and lowest stage of 6 °C was optimal with a 15.1% reduction in charging time compared to a single-stage one. Although the cooling capacity and exergy stored in cascaded cold storage were less than those in a single-stage one, the charging rate and exergy efficiency were dramatically increased (Cheng & Zhai, 2018b). It was also found by Li et al. (B. Li et al., 2019), through a one-dimensional transient model of a cascaded packed-bed cold storage, that the multiple stages made the phase change process faster and more uniform. Second, the internal structure of PCM capsules has been optimized. Jia et al. (Jia et al., 2019) carried out an experimental and numerical study on a spherical PCM capsule with circular pin-fins, in terms of the internal temperature, liquid fraction and charging rate of capsules with various pin-fin configurations. It was found that the charging rate was improved dramatically by adding fins, and the charging time was decreased by >50% in capsule with six fins compared to that without fins. Third, novel geometric structures of PCM capsules have been proposed. An innovative red blood cell (RBC) shaped PCM capsule was studied by Cheng et al. through experiment and simulation (Cheng & Zhai, 2017). Its thermal performance was compared to that of various deformation structures, e.g. cylinder, drum, ring and sphere. The results revealed that the RBC-shaped capsule had the best thermal performance.

In the following work (Cheng et al., 2020), forced convection of external flows over an RBC-shaped PCM capsule was numerically studied in a steady-state laminar flow region. It was found that the drag coefficient of the capsule decreased with the increase of Reynolds number. 0° attack angle was recommended for the RBC-shaped capsule for its low drag force and high Nusselt number. The last aspect of packed-bed cold storage studies is the capsule layout and configuration in the packed bed to improve the fluid flow and thermal performances in the packed beds. Halkarni et al. (Halkarni et al., 2017) estimated the local wall heat transfer coefficient by infrared (IR) thermography in the packed beds randomly filled with uniformly sized spheres. Lee and Chung (Lee & Chung, 2019) experimentally investigated the forced convective heat transfer across heated spheres in packed beds. The results indicated that the Nusselt number decreased as the ratio of bed height to sphere diameter increased due to the axial dispersion. Zenner et al. (Zenner et al., 2019) presented a new robust experimental setup and demonstrated that the size of the cylinder and the diameter of the inner holes were central to generalizing the thermal performance and the pressure drop in the packed bed. Yeboah and Darkwa (Yeboah & Darkwa, 2019) compared a Z-annular flow configuration and conventional packed beds of the same dimension. It was concluded that the Z-annular flow configuration had the potential to enhance the heat transfer and storage capacity. Guo et al. (Guo et al., 2019) constructed a free channel, flow guiding conduit (FGC), in the center of a packed bed using highly fluid-penetrable material, thus promoting flow in the lateral direction with Venturi effect. According to the results, the capsule layout plays a significant role in the hydrodynamic and heat transfer performance in real applications.

To date, randomly packed beds have witnessed substantial efforts in the literature to improve their flow and heat transfer performances. Halkarni et al. (Halkarni et al., 2016) used a transient technique to measure volumetric heat transfer coefficient in randomly packed beds with uniformly sized spheres. There was an increase in the volumetric heat transfer coefficient with the increase in Reynolds number. Das et al. (Das et al., 2017) presented a fully resolved direct numerical model of a slender random packed-bed reactor.

Correlations of the pressure drop and the overall heat transfer coefficient were proposed. It was seen that the pressure drops in randomly packed beds were reduced largely and the corresponding heat transfer performance was improved by the superior configurations. Guo and Dai (Guo & Dai, 2010) presented a fully resolved direct numerical model of a slender randomly packed bed and found the fully resolved accurate numerical simulations helped toelucidate detailed pore-scale flow and heat transfer features. Calis et al. (Calis et al., 2001) set up a randomly packed pebble bed test facility and proposed a new correlation to predict the pressure drop and convective heat transfer characteristics in the bed. However,

inevitable shortcomings were noticed in random packing systems as the pressure drop was typically far higher than other packing forms. Moreover, it is evident that the flow and heat transfer distribution is inhomogeneous in such packed beds, and it is difficult to predict the location of the hotspot (Sobes et al., 2011).

To address the above issues, structured packed beds are proposed instead of traditional randomly packed beds. Calis et al. (Calis et al., 2001) and Romkes et al. (Romkes et al., 2003) compared the thermal-hydraulic performance of five packing forms of composite structured packed beds both numerically and experimentally. The results revealed that the pressure loss was reduced remarkably and the heat transfer characteristics were affected greatly by means of composite structured packing. Qian et al. (Qian et al., 2019) proposed a kind of grille-sphere composite packed bed and found that the pressure drop was decreased and the radial heat transfer performance was increased compared with a randomly packed bed. Guo et al. (Guo et al., 2017; Guo et al., 2019) proposed a kind of slender packed beds with novel packing layouts, where particles in contact with the wall tended to form a highly ordered ring structure, thus rendering the pressure drop decreased and heat transfer efficiency enhanced to some extent. Tian et al. (Tian et al., 2018) experimentally explored fluid flow and heat transfer characteristics of power-law fluid in wall-bounded three-dimensional structured packed beds of spheres. The relationship between the pressure drop and flow velocity was verified by modified Ergun type equations. Guo et al. (Guo et al. , 2019) studied the effects of the confining wall on particle-to-fluid convective heat transfer and pressure drop, and found two different flow distributions in the packed beds, i.e. the wall-channeling type and the regular-packing-dominating type. Toghraie et al. (Toghraie et al., 2018) investigated wall effects on the cross and axial flow and heat transfer of particles in a packed bed and found that heat transfer improved as the particle moves closer to the wall.

To further analyze effects on thermal-hydraulic performance affected by capsule layout, Hu et al. (Hu et al., 2019; Hu et al., 2018) and Wang et al. (Wang et al., 2018) classified the packing configuration into three types, including simple cubic (SC), body-centered cubic (BCC) and face-centered cubic (FCC) ones. The simulation and experimental work on the flow and heat transfer characteristics were extensively carried out in the packed beds with internal spherical particles and external rectangular tanks. It was found that these novel structures had a remarkable capability for decreasing pressure loss and enhancing heat transfer efficiency, echoed by Guo et al. (Guo et al., 2019) and Chen et al. (Chen et al., 2017).

Despite the reduced pressure loss of loose packed-bed layouts, it is noted that these packed beds are featured by large volume size and high manufacturing cost of the tank due to their high porosity and low energy storage density. It may limit the implementation of PCM packed beds (T. Li et al., 2019). On the other hand, to the best of our knowledge, the existing investigation on packing structures mainly focuses on rectangular containers, while the arrangements of spheres in cylindrical ones, which are more suitable for PCM cold storage, are rarely mentioned in the literature. Compared to rectangular configurations, cylindrical packed beds offer distinct advantages for PCM cold storage, including inherent structural robustness to withstand thermal and mechanical stresses, radial symmetry for uniform heat distribution, and compactness that minimizes surface-area-to-volume ratios and thermal losses. Their geometry aligns naturally with industrial standards for pressurized systems, enabling seamless integration into real-world applications such as HVAC and thermal energy storage units. Furthermore, the concentric arrangement of capsules in cylindrical beds enhances packing density and flow uniformity, addressing critical challenges in scalability and thermal performance. To overcome the issues of large packed bed volume, this study was inspired by the arrangement of atoms or ions in metal and ionic lattices, which can be geometrically regarded as packing of uniform spheres, where crystals tend to lie in the most stabilized or lowest internal energy state (Grosso & Parravicini, 2013).

From this perspective, spheres get as close to each other as possible, thus occupying the minimum space. Based on the closest packing principle of crystal structures, two novel packing configurations of spherical capsules, i.e. FCC (same as aforementioned) and hexagonal closest packed (HCP), are proposed in the present study for cylindrically packed-bed PCM cold storage. Through a numerical study using ANSYS Fluent 18.0, the hydrodynamic and heat transfer performances of these two packed forms are comprehensively compared with that of the conventional ADL packing layout. First, the transient thermal performances and pressure loss in the whole packed beds with different capsule layouts were studied during PCM solidification, to examine the advantages of diverse packing configurations in cold storage applications. In addition, the power consumption together with a self-developed new metric, the normalized charging efficiency factor, were employed to evaluate the three packing configurations, which provided important advancement of knowledge to future studies.

2. Numerical methods

2.1. Physical model of packed-bed cold storage tank

As illustrated in **Fig. 1** (a), the 171 spherical PCM capsules with an identical inner radius of 20 mm, with a shell thickness of 1 mm, were stacked sequentially in a conventional cylindrical packed bed (ADL) with an inner diameter of 220 mm (including gaps between capsules) and a rated cold storage capacity identical to 576.3 kJ. The capsules were divided into nine layers with 19 capsules in each layer. Water, as the heat transfer fluid (HTF), flew into the packed-bed tank from the bottom to the top during the charging process as a laminar steady flow. Based on this configuration, two typical dense packing configurations of the cold storage tank, i.e. the HCP and FCC layouts, were developed as schematically depicted in **Fig. 1** (b) and (c) respectively, with the same number of capsules in the tank and in each layer. As can be seen, in the HCP and FCC layouts, the three-dimensional arrangements consisted of stacks of packing layers that were closer to each other, in which any three adjacent spheres composed

an equilateral triangle. In other words, each sphere had 12 spheres contacting it tangentially. The number of tangential spheres of each capsule in the ADL packing was only eight. It was noted that the height of FCC and HCP packing was 316 mm while the height of ADL packing was 378 mm.

The PCM selected for the present study was a composite organic PCM, capric acid – lauric acid – oleic acid (CA-LA-OA), which has an appropriate phase change temperature for cold storage of air-conditioning systems (Wang et al., 2013). This PCM was self-developed and has manifested excellent thermal performance in a former study (Wang et al., 2019). Since the phase change of the PCM proceeded within a small temperature range, the influence of the slightly varied density and thermal conductivity on the phase change process was assumed negligible. The thermal-physical properties were treated as temperature independent as listed in **Table 1** (Guo et al., 2019; Wang et al., 2019). Water was selected as the HTF, which had a constant flowrate of 100 $L \cdot h^{-1}$ and a constant inlet temperature of = 7 °C. The initial temperature of the packed bed was uniform and set as = 22 °C.

2.2. Governing equations and numerical methods

In this work, a three-dimensional simulation model was established to describe the transient phase change process accompanied by the forced convection of HTF. The following assumptions were made:

1) The flow in the packed bed is steady and incompressible;

2) The thermal resistance of capsule shell is ignored considering that the capsule shell was set as thin as 1 mm and the shell thermal conductivity was 2.20 $W \cdot m^{-1} \cdot K^{-1}$, the effect of which was proven negligible (Wang et al., 2013);

3) The envelope is modeled as a rigid layer, and the effect of deformation is ignored in the simulation as Reynolds number is so low that the fluid can hardly cause any deformation of capsules;

4) PCM is homogeneous and isotropic;

5) Natural convection inside PCM capsules is neglected due to the small temperature difference ($\Delta T = 15°C$) between HTF and PCM, minimal density variation (~0.6%) between solid and liquid phases, and the conduction-dominated regime in small capsules (radius = 20 mm). This assumption is further justified by the low Rayleigh number ($Ra < 10^3$), which suppresses buoyancy-driven flows, as corroborated by prior studies (Ismail & Henríquez, 2000; Kenisarin et al., 2020; Sheikholeslami, 2018);

6) Gravitational force, as well as other external body forces, are neglected.

Based on the assumptions, for HTF the conservation equations of mass, momentum and energy are formulated as follows:

$$\frac{\partial(u_i)}{\partial x_i} = 0 \tag{1}$$

$$\rho_f \frac{\partial u_i}{\partial t} + \rho_f \frac{\partial}{\partial x_j}(u_i u_j) = -\frac{\partial P}{\partial x_i} + \mu_f \frac{\partial^2 u_i}{\partial x_j \partial x_j} \tag{2}$$

$$\rho_f c_f \frac{\partial T_f}{\partial t} + u_i \rho_f c_f \frac{\partial T_f}{\partial x_i} = k_f \frac{\partial^2 T_f}{\partial x_i \partial x_i} \tag{3}$$

where T_f is the temperature of the fluid, and k_f is the fluid thermal conductivity, and i represents a spatial coordinate direction in a Cartesian coordinate system.

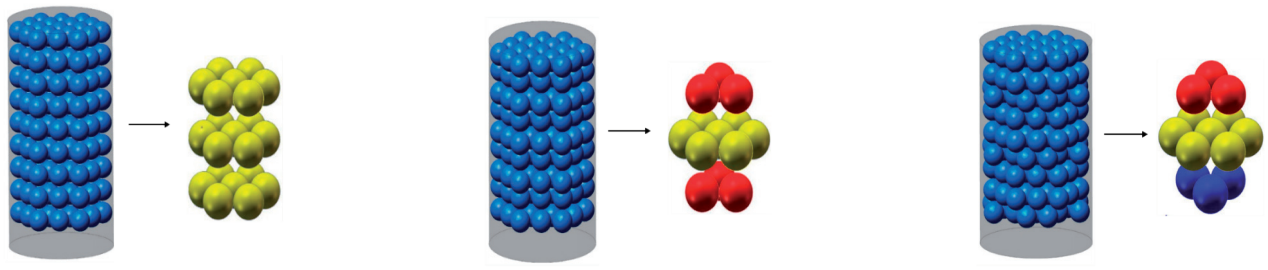

(a) (b) (c)

Fig. 1. Schematic of packed-bed cold storage: (a) ADL layout, (b) HCP layout, and (c) FCC layout

Table 1. Thermal-physical properties of the PCM and HTF

Material	state	ρ ($kg \cdot m^{-3}$)	c ($J \cdot kg^{-1} \cdot K^{-1}$)	k ($W \cdot m^{-1} \cdot K^{-1}$)	T (°C)	ΔH ($kJ \cdot kg^{-1}$)
C-L/O PCM	solid	845.1	1825	0.145	10.5	109.2
	liquid	839.7	2214	0.141	14.5	
HTF (water)	liquid	999.7	4193	0.58	-	-

For PCM, the enthalpy method was adopted to express the phase change process, by which one does not need to track the movement of solid-liquid phase interface during solidification/melting. The total enthalpy H consists of the sensible enthalpy h and the latent heat ΔH:

$$H = h + \Delta H \tag{4}$$

$$h = h_{\mathrm{ref}} + \int_{T_{\mathrm{ref}}}^{T} c_{\mathrm{p}} \mathrm{d}T \tag{5}$$

$$\Delta \mathrm{H} = \gamma L \tag{6}$$

where h_{ref} and T_{ref} are the reference enthalpy and temperature of the PCM, while c_{p} and L represent the specific heat and the latent heat of PCM, respectively. The liquid fraction γ is defined in Eq. (7) as:

$$\gamma = \begin{cases} 0 & \left(T_{\mathrm{p}} < T_{\mathrm{solidus}}\right) \\ \frac{T_{\mathrm{p}} - T_{\mathrm{solidus}}}{T_{\mathrm{liquidus}} - T_{\mathrm{solidus}}} & \left(T_{\mathrm{solidus}} < T_{\mathrm{p}} < T_{\mathrm{liquidus}}\right) \\ 1 & \left(T_{\mathrm{p}} > T_{\mathrm{liquidus}}\right) \end{cases} \tag{7}$$

As a result, the energy equation for the PCM region is formulated as:

$$\rho_{\mathrm{p}} \frac{\partial H}{\partial t} = k_{\mathrm{p}} \frac{\partial^2 T_{\mathrm{p}}}{\partial x_{\mathrm{i}} \partial x_{\mathrm{i}}} \tag{8}$$

where T_{p} is the temperature of the PCM and k_{p} is the PCM thermal conductivity.

The Reynolds number for this model, as Eq. (9) shows, is based on the interstitial velocity v_{i} and the pore-scale hydraulic diameter d_{h} of the packed bed (Yang et al., 2010).

$$Re_{\mathrm{h}} = \frac{\rho_{\mathrm{f}} v_{\mathrm{i}} d_{\mathrm{h}}}{\mu_{\mathrm{f}}} \tag{9}$$

where ρ_{f} and μ_{f} are the density and dynamic viscosity of water, respectively, while the interstitial velocity v_{i} and the pore-scale hydraulic diameter d_{h} are defined by Eq.10 and Eq.11 respectively:

$$v_{\mathrm{i}} = \frac{v_{\mathrm{s}}}{\varphi} \tag{10}$$

where v_s is the inlet flow velocity, and φ is the porosity of the packed bed, that is also the proportion of space taken by HTF in the packed bed. The detailed φ values of ADL, HCP and FCC are 39.5%, 26.0% and 26.0%.

$$d_{\mathrm{h}} = 4 \frac{\varphi}{1-\varphi} \cdot \frac{V_{\mathrm{p}}}{A_{\mathrm{p}}} \tag{11}$$

where V_{p} and A_{p} are the volume and surface area of the capsule.

The surface average Nusselt number is defined as:

$$Nu_{aver} = \frac{q_s d_h}{(\overline{T_f} - \overline{T_s}) k_f} \tag{12}$$

where q_{s} is the heat flux of the active ball; $\overline{T}_{\mathrm{f}}$ is the volume average temperature of HTF; and $\overline{T}_{\mathrm{s}}$ is the surface average temperature of the active ball.

As for PCM packed beds, both pressure drop and heat transfer contribute to the thermal efficiency and they should be taken into account simultaneously. The improvement of heat transfer is usually at the cost of increased pressure drop. To evaluate the heat transfer performance considering both factors, the thermal performance factor to evaluate the heat transfer enhancement in the work (Gong et al., 2015) is defined below:

$$\mathrm{JF} = \left(\frac{Nu}{Nu_{ADL}}\right) / \left(\frac{\Delta p / L}{(\Delta p / L)_{ADL}}\right)^{1/3} \tag{13}$$

where Nu_{ADL} and $(\Delta p / L)_{ADL}$ are respectively the Nusselt number and pressure drop of the ADL packing.

2.3. Meshing and implementation

The collinear geometric packing configuration of spherical capsules brings about point contacts in the form of sphere-sphere and sphere-wall interaction in the packed bed, where the mesh quality tends to be poor. Therefore, four methods, i.e. reducing, overlapping, caps and bridges, have been proposed in the literature to modify the contact point (Rebughini et al., 2016). Reported by Calis et al. (Calis et al., 2001), the reducing method, in which the spheres are stacked with very small gaps (1% of capsule outer radius) without contacting, was employed in the present study. The unstructured grids with tetrahedral elements were adopted for mesh generation in the domain due to their complicated geometric structures. **Fig. 2** shows a typical mesh distribution, where the grids near spherical surfaces are intensified.

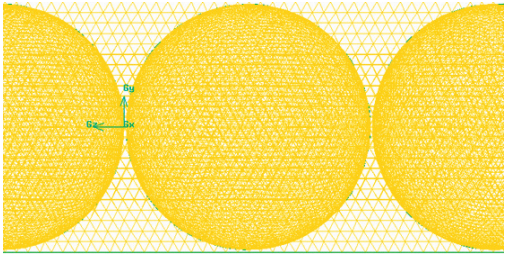

Fig. 2. Computational grid of the ADL layout model

The modelling was performed using the commercial software of ANSYS Fluent 18.0. The Reynolds numbers in the present study ranged from 1 to 200. The Energy model was turned on, and the steady-state laminar flow model was used as the momentum equation for this simulation. The SIMPLE algorithm was adopted for the pressure-velocity coupling. The Green-Gauss cell-based scheme was applied for the gradients, the stand discretization scheme was imposed on the pressure equation, and the second-order upwind scheme was selected for the momentum and energy equations. The convergence criteria were determined by monitoring the convergence residual for the continuity, momentum, and energy equations, which are set to 10^{-3}, 10^{-6}, and 10^{-6}, respectively.

2.4. Initial and boundary conditions

For the physical model of the packed-bed cold storage tank, the computation domains consisted of both the PCM capsules and the HTF. The initial temperature, T_{ini} for the whole packed bed was 22 °C and the initial velocity of HTF, u_{ini}, was 0. The coupled thermal boundaries were imposed on capsule surfaces in these cases. The inlet temperature, T_{in}, was set to 7 °C and a wide range of Reynolds numbers from 1 to 200 were investigated. The pressure condition of 0 Pa gauge backflow pressure was applied at the outlet. All the surfaces were set as no-slip walls.

3. Grid independence test and model validation

3.1. Independence of model grid and time step

Prior to iterative computations, grid size and time step convergence were checked. The total pressure drop and transient liquid fraction were selected as two typical metrics to test three different mesh sizes and time steps for the case of the packed-bed model with ADL layout. **Table 2** reveals the variations of the two metrics for the case among different mesh sizes and time steps. It can be recognized that a grid size of approximately 300000 cells and a time step of 0.1 s, which satisfied 0.8 of maximum skewness with a low aspect ratio, can be an ideal option considering both the accuracy and computational time. Similarly, the mesh sizes and time steps for other cases were examined. The corresponding mesh quality was also tested on the condition of no more than 0.85 of maximum skewness and 5.0 of maximum aspect ratio. The total numbers of grid elements for all the cases are listed in **Table 3**.

3.2. Experimental validation

Experimental tests were performed to validate the mathematical model. As shown in **Fig. 3**, the main experimental system consisted of a thermostated water bath and a chilled-water packed-bed cold storage tank. The cold storage tank was placed horizontally, and water that served as HTF was pumped to the inlet during the charging process. Nine layers with 19 capsules in each layer were packed in the storage tank. The PCM capsules were filled with composite C-L/O PCM. The capsule diameter and capsule wall thickness were 20 mm and 0.3 mm, respectively. The storage tank was insulated with a 4-cm rubber foam insulation layer.

To log water temperature and PCM temperature variation, 28 PT100 temperature sensors were fixed at different bed heights and seven-layer PT100 temperature sensors were equidistantly placed in the packed bed. At each layer, 4 PT100 temperature sensors were used to monitor HTF temperature and PCM temperature at the center of the spherical capsules. The first layer near the bottom of the bed and the last layer near the top of the bed were designated as the inlet and outlet of the packed bed. A rotameter with an accuracy of ±4% was employed to monitor the flow rate. All the PT100 sensors, with an accuracy of ±0.15 °C, were calibrated using the thermostatic water bath. The temperature was logged every 30 s by the Keithley 2700 data acquisition system.

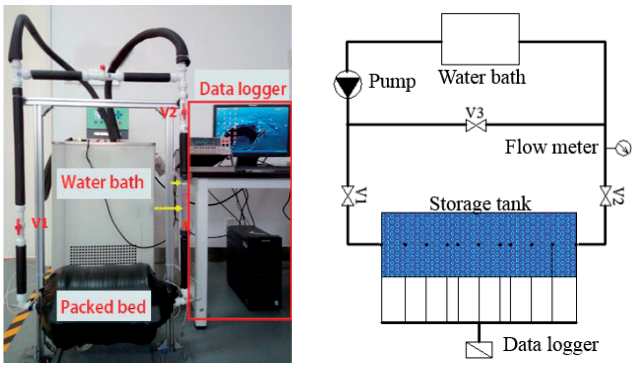

(a) (b)

Fig. 3. Experimental setup: (a) photo of the experimental setup; (b) schematic of the experimental setup

Numerical predicted time-dependent variations of HTF and PCM temperature were compared with the experimental data. The flow rate was 100 L h^{-1} and the inlet temperature was 7 °C. Root mean square error (RMSE) and Mean Absolute Percentage Error (MAPE) were used to evaluate the deviations between the simulation results and experimental data.

$$\mathrm{RMSE} = \sqrt{\frac{1}{n}\sum_{\tau=1}^{n}(T_\tau - T_\tau')^2} \quad (4)$$

$$\mathrm{MAPE} = \frac{1}{n}\sum_{\tau=1}^{n}\left|\frac{T_\tau - T_\tau'}{T_\tau'}\right| \quad (5)$$

where n is the total number of data compared. T_τ and T_τ' are the simulated and experimental temperature, respectively, recorded at the time step of τ.

The comparison of experimental and simulated PCM and HTF temperatures are shown in **Fig. 4**. The simulation results are in good agreement with the experimental data, as the RMSE and MAPE for the PCM temperature are observed to be 0.89 °C and 5.49%, and the corresponding values for HTF temperature are 0.41 °C and 2.04%.

Table 2. Grid size and time step independence test result for the packed-bed model with ADL layout

Number of cells	Time step (s)	Δp_{total}(Pa/m)	Liquid fraction		
			1000 s	5000 s	10000 s
1,035,976	0.1	0.0455	0.8592	0.3825	0.1312
1,223,391	0.1	0.0461	0.8578	0.3807	0.1305
1,979,355	0.1	0.0464	0.8577	0.3796	0.1301
1,223,391	0.05	0.0461	0.8578	0.3812	0.1307
1,223,391	0.1	0.0461	0.8578	0.3807	0.1305
1,223,391	0.2	0.0462	0.8578	0.3789	0.1296

Table 3. Grid size and time step independence test result for different models

Case	ADL	HCP	FCC
Number of grid elements	1,223,391	3,003,764	3,006,938
Time step (s)	0.1	0.1	0.1

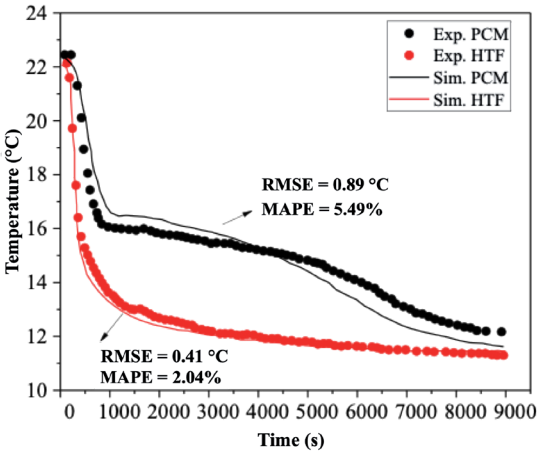

Fig. 4. Comparisons of experimental data with numerical results

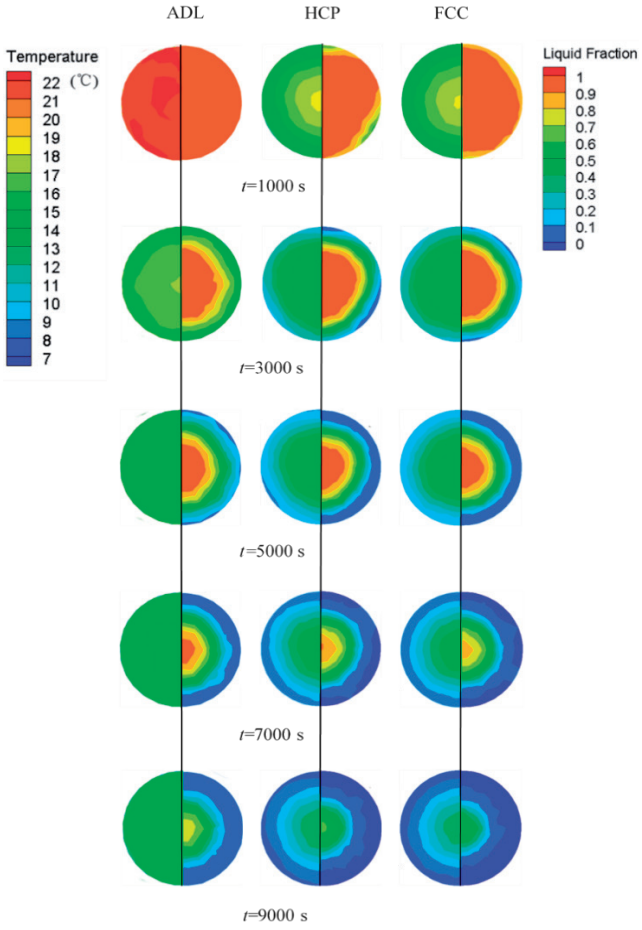

Fig. 5. Temperature gradient (left half) and liquid fraction distribution (right half) of the capsule cross section ($z = 0$) of different packed-bed model packing configurations

4. Results and discussion

4.1. Effects of the packing configuration on the packed bed

Considering the compactness, compared with the ADL packing, the theoretical PCM packing density for HCP and FCC layouts was raised by 22.5%, thus considerably saving the footprint of the packed bed. Furthermore, the packing density compares favorably with other recent strategies aimed at improving thermal performance. For example, in a study involving hydrate-based carbon capture using packed RBC-shaped capsules (Zhang et al., 2024), the reported packing density was 64.3%, which is approximately 13% lower than that of the HCP and FCC layouts. In addition, studies utilizing flow-guiding conduits have generally resulted in lower packing densities due to the volume occupied by internal structures within the packed bed (Guo et al., 2019).

Based on the investigation of flow and heat transfer mechanisms of different packing configurations in the model of a whole packed bed, a practical analysis of the charging rate across the different packed beds was carried out. The PCM mass and inlet HTF flowrate (100 L/h) were identical for all the packing configurations to make sure that the layout is the only variable. All the capsules in the packed bed were active to exchange heat with HTF. The parameters and boundary conditions of the packed beds are depicted in Section 2.1. The capsule in the center of the fifth layer was selected as an example to represent the charging process of the packing configuration. **Fig. 5** depicts the temperature gradient (left half) and liquid fraction distribution (right half) of the cross section (z = 0) of the selected sphere.

The comparisons are implemented at several typical time instants. For t = 1000 s, the temperature was at a uniform level of 21 °C throughout the sphere in ADL. The heat transfer was attributed to pure heat conduction. In regard to the other two packed beds, the isotherms presented as a series of concentric circles. Regarding the phase change process, the liquid fraction distribution in FCC was more homogeneous than in HCP. This means that the melting front in FCC progressed more uniformly across the sphere, with smaller local variations in the liquid fraction, whereas HCP showed greater disparities in the liquid fraction, indicating less uniform phase change behavior. At t = 3000 s, PCM in ADL began to solidify, while its solidification rate was the slowest. The phase change process in the center of spheres lagged behind other domains due to the highest thermal resistance. Beyond t = 7000 s, almost all the PCM in the sphere of HCP and FCC began to solidify; however, a small portion of PCM at the sphere center of ADL did not begin to solidify before t = 9000 s.

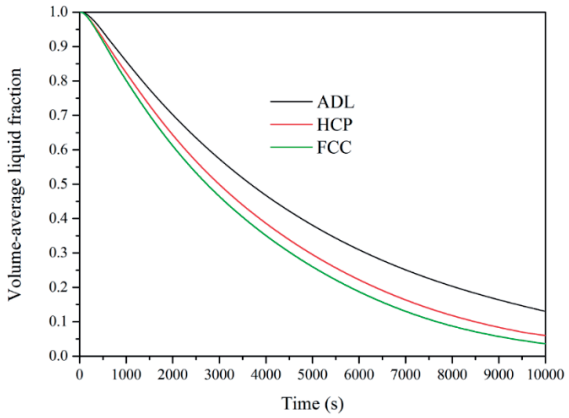

Fig. 6. Variation of PCM volume-average liquid fraction of different packed-bed model packing configurations

A key index, the volume-average liquid fraction of PCM, is employed to assess the thermal performance of each packed bed. As the volume-average liquid fraction declines from 1 to 0, it indicates that PCM in the packed bed gradually changes its phase state towards the complete solid. **Fig. 6** shows the variation of PCM volume-average liquid fraction in different cases. It was observed that the liquid fraction distribution in each packed bed presented a similar downtrend, while the duration of the charging process decreased in the order of ADL > HCP > FCC. To analyze the peculiarity of transient solidification rate quantitatively, the charging time is defined in this study as the minimum time required for PCM in the packed bed to reach 90% phase change. It was revealed that HCP and FCC saved up to 21.4% and 29.0% of charging time, respectively, in comparison with that of ADL. The results suggest that the overall heat transfer capability of HCP and FCC is greatly improved during solidification and the increased extent of FCC is more dramatic.

To figure out the heat transfer performance during the charging period in each packed bed, the variations of charging rates of different cases are shown in **Fig. 7**. It was displayed that the cold storage process in diversely packed beds could be divided into three successive stages. In the initial sensible cooling stage (0–300 s), the large temperature gradient between the HTF and PCM drives rapid sensible heat extraction. Convective heat transfer at the capsule surfaces dominates, with no phase change occurring. The charging rate rises sharply to a peak value (~50 W difference between FCC and ADL at t = 300 s), reflecting enhanced convective efficiency in structured layouts (FCC/HCP) due to reduced flow channeling. In the latent heat release stage (300–4500 s), solidification initiates at the capsule periphery as PCM temperatures reach the phase change point. Latent heat release stabilizes local temperatures, while thermal resistance from the growing solid layer gradually reduces the charging rate. The FCC layout accelerates this stage by minimizing void spaces, which enhances HTF-PCM contact and convective heat transfer. In the final sensible cooling stage (t > 4500 s), residual heat is removed via conduction through the solid phase. The diminished temperature gradient results in a slow, monotonic decline in charging rates. Notably, the charging rate order reverses beyond 4500 s, as ADL's looser packing allows marginally better conduction in the fully solidified regime.

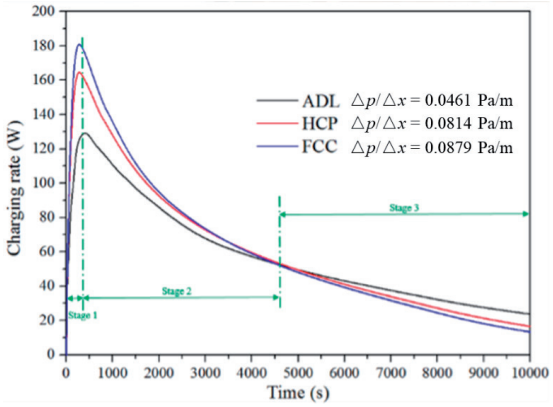

Fig. 7. Transient variations of charging rate and pressure drop of different packed-bed model packing configurations

However, despite improving heat transfer rate, the pressure drop across the whole packed bed inevitably increased in the cases of HCP and FCC. The time-independent flow of HTF in the packed resulted in the pressure drops of ADL, HCP and FCC of 0.0461, 0.0814 and 0.0879 Pa m^{-1}, respectively. I.e., the optimized packing configura-

tions played a significant role in enhancing heat transfer efficiency of the whole packed bed, however at the cost of increased pressure drop. While FCC/HCP layouts incur higher pressure drops, their superior thermal performance and compactness result in net energy savings and reduced system footprint.

A comparative analysis of different packed bed configurations in terms of energy storage density, heat transfer enhancement, and pressure drop characteristics is shown in **Table 4**. Studies on grille-sphere composite packed beds (GSCSPBs) have shown that their particle-to-fluid heat transfer coefficient is 94% higher than that of simple cubic (SC) packing, reaching approximately 76% of the heat transfer observed in randomly packed beds (Wang et al., 2017). Meanwhile, composite structured packed beds (CSPBs) exhibit improved heat transfer due to enhanced flow distribution and increased fluid-solid contact areas while maintaining a lower pressure drop than randomly packed beds (Romkes et al., 2003). In contrast, the HCP and FCC layouts provide a high packing density (~74%), which translates to increased energy storage capacity, while also offering structured conduction pathways for thermal enhancement. Although GSCSPBs and CSPBs focus on optimizing heat transfer and flow resistance, their energy storage density is generally lower, making HCP and FCC configurations more suitable for applications prioritizing thermal storage efficiency.

4.2. Normalized charging efficiency factor of packed bed cold storage

The newly defined normalized charging efficiency factor, β_{charge}, is formulated in Eq (16). Differing from the overall thermal performance factor, this metric compares the cooling capacity storage gain to the pump hydraulic power. It is defined as the ratio of the average charging rate (the gain) to the (modified) pressure loss (the cost). Due to the fact that the pump power consumption usually accounts for a small portion of the chiller power consumption, the ratio between the two is used to modify the weight of pressure loss as an exponential:

$$\beta_{\text{charge}} = \frac{E_{\text{charge}} / \tau}{\Delta p^{Q_{\text{pump}}/Q_{\text{charge}}}} = \frac{E_{\text{charge}} / \tau}{\Delta p^{(\frac{q\Delta p}{1000\eta})/(\frac{E_{\text{charge}}/\tau}{\text{COP}})}} \tag{16}$$

where E_{charge} (J) is the overall cooling capacity of the packed-bed cold storage; COP refers to the coefficient of performance of the chiller; q is the HTF flowrate (L s^{-1}); Δp is the overall pressure loss of the packed-bed cold storage (Pa); τ and η are the time and the lumped pump and motor efficiency (%), respectively. The pump electric power, Q_{pump} (W) may be calculated using the formula below (Karassik, 2001).

Table 4. Comparative Analysis of Packing Configurations

Packing Configuration	Energy Storage Density	Heat Transfer Enhancement	Pressure Drop Characteristics
Hexagonal Close-Packed (HCP)	High (≈74% packing density)	Moderate; improved conduction pathways due to ordered structure.	Moderate; increased contact points may lead to higher pressure drop compared to less dense packings.
Face-Centered Cubic (FCC)	High (≈74% packing density)	Moderate; similar to HCP with efficient conduction pathways.	Moderate; structured arrangement balances pressure drop and heat transfer.
Composite Structured Packed Beds (CSPBs) (Romkes et al., 2003)	Moderate to High; specific values not detailed in literature	Enhanced; improved flow distribution and increased contact area between fluid and particles.	Reduced compared to randomly packed beds;
Grille-Sphere Composite Packed Beds (GSCSPBs) (Wang et al., 2017)	Moderate to High; specific values not detailed in literature	Significantly enhanced; studies report up to 94% higher heat transfer coefficients compared to simple cubic packing and achieving 76% of the heat transfer in randomly packed beds.	Lower than randomly packed beds

Table 5. Key performance metrics of the whole packed bed with three packing configurations

Packing configuration	Charging time (s)	Total pressure loss (Pa)	Energy storage density (%)	Pump power consumption (W)	Normalized charging efficiency factor
ADL	10.8×10^3	0.0166	60.5	8.39	68.0
HCP	8.49×10^3	0.0245	74.1	6.70	83.5
FCC	7.67×10^3	0.0265	74.1	6.48	91.6

$$Q_{\text{pump}} = \frac{q\Delta p}{1000\eta} \quad (17)$$

The simulation result of charging time and pressure loss are summarized in **Table 5** for the case of ADL, HCP and FCC. The total cooling capacity was 576,304 J. COP in this study was set at 5, and the pump efficiency and motor efficiency were both 0.85. They were all the same for the three cases. The charging time of the whole packed-bed cold storage was reduced by 21.4% and 29.0% by applying HCP and FCC configurations, respectively, in comparison to ADL. Based on the aforementioned flow parameters, the pump power consumption was calculated considering both pressure loss and gravity. The results showed that FCC also consumes the lowest pumping power due to the shortest charging time and small height. The normalized charging efficiency factor, as defined, compares the rate of charging with the cost of pumping power. From the results, FCC achieved the best efficiency (34.7% higher than that of ADL), followed by HCP (22.8% higher than that of ADL). Dense packings are better performing in all the metrics than loose capsule packings.

5. Conclusions

In the present paper, two new packing configurations of capsules, FCC and HCP, were designed for the PCM packed-bed cold storage to increase the storage density. Through simulation conducted in ANSYS Fluent 18.0, the flow characteristics and heat transfer performance of the packed bed with various capsule packings were investigated and compared at different Reynolds numbers. The conclusions are as follows:

(1) HCC and FCC are both three-dimensional dense packings, which plays a vital role in saving space volume and manufacturing costs for PCM packed beds. By comparison, the theoretical PCM packed density of HCP and FCC packing is 22.5% larger than that of conventional ADL packing.

(2) Compared with other packings, FCC, despite its improved heat transfer performance, inevitably exhibits the increased pressure drop across the whole packed bed. The pressure drop of ADL, HCP and FCC is 0.0461, 0.0814 and 0.0879 Pa m^{-1}, respectively.

(3) As for PCM packed beds, the charging time of the packed-bed cold storage is reduced by 21.4% and 29.0% by applying HCP and FCC configurations, respectively, compared to ADL. It is found that FCC bed has superior heat transfer rates due to promoted convection in HTF.

(4) A new metric, normalized charging efficiency factor, was defined for the first time, comparing the cooling capacity storage gain to the pump hydraulic power. The best value was found for FCC (34.7% higher than that of ADL), followed by HCP (22.8% higher than that of ADL).

While the FCC and HCP layouts demonstrate superior thermal performance and energy density for PCM cold storage, their commercial adoption faces challenges, including manufacturing complexity, scalability constraints and maintenance challenges. However, the principles of structured packing offer valuable insights transferable to diverse fields. Applications such as solar thermal energy storage, catalytic and biomedical reactors, can leverage optimized packing geometries to enhance heat transfer, reduce footprint, and balance hydraulic-thermal trade-offs.

Acknowledgements

This work was supported by the National Natural Science Foundation of China under contract No. 51776117.

Reference

Bindra, H., Bueno, P., Morris, J. F., & Shinnar, R. (2013). Thermal analysis and exergy evaluation of packed bed thermal storage systems. *Applied Thermal Engineering*, *52*(2), 255-263.

Calis, H., Nijenhuis, J., Paikert, B., Dautzenberg, F., & Van Den Bleek, C. (2001). CFD modelling and experimental validation of pressure drop and flow profile in a novel structured catalytic reactor packing. *Chemical Engineering Science*, *56*(4), 1713-1720.

Chen, L., Lee, W., & Lee, J. (2017). Analysis of the thermal field and heat transfer characteristics of pebble beds packed in a face-centered cubic structure. *Applied Thermal Engineering*, *121*, 473-483.

Chen, L., Wang, C., Moscardini, M., Kamlah, M., & Liu, S. (2019). A DEM-based heat transfer model for the evaluation of effective thermal conductivity of packed beds filled with stagnant fluid: Thermal contact theory and numerical simulation. *International Journal of Heat and Mass Transfer*, *132*, 331-346.

Cheng, X., & Zhai, X. (2017). Thermal performance analysis of a novel PCM capsule in red blood cell shape. *Applied Thermal Engineering*, *120*, 130-137.

Cheng, X., & Zhai, X. (2018a). Thermal performance analysis and optimization of a cascaded packed bed cool thermal energy storage unit using multiple phase change materials. *Applied Energy*, *215*, 566-576.

Cheng, X., & Zhai, X. (2018b). Thermal performance analysis of a cascaded cold storage unit using multiple PCMs. *Energy*, *143*, 448-457.

Cheng, X., Zhai, X., Wang, X., & Lin, P. (2020). Numerical study of forced convection over phase change material capsules in a traditional spherical shape and a biomimetic shape. *Journal of Energy Storage*, *31*, 101526.

Das, S., Deen, N. G., & Kuipers, J. (2017). A DNS study of flow and heat transfer through slender fixed-bed reactors randomly packed with spherical particles. *Chemical Engineering Science*, *160*, 1-19.

Diao, Y., Liang, L., Zhao, Y., Wang, Z., & Bai, F. (2019). Numerical investigation of the thermal performance enhancement of latent heat thermal energy storage using longitudinal rectangular fins and flat micro-heat pipe arrays. *Applied Energy*, *233*, 894-905.

Fleuchaus, P., Godschalk, B., Stober, I., & Blum, P. (2018). Worldwide application of aquifer thermal energy storage–A review. *Renewable and Sustainable Energy Reviews*, *94*, 861-876.

Gielen, D., Boshell, F., Saygin, D., Bazilian, M. D., Wagner, N., & Gorini, R. (2019). The role of renewable energy in the global energy transformation. *Energy strategy reviews*, *24*, 38-50.

Gong, B., Wang, L.-B., & Lin, Z.-M. (2015). Heat transfer characteristics of a circular tube bank fin heat exchanger with fins punched curve rectangular vortex generators in the wake regions of the tubes. *Applied Thermal Engineering*, *75*, 224-238.

Grosso, G., & Parravicini, G. P. (2013). *Solid state physics*. Academic press.

Guo, X., & Dai, R. (2010). Numerical simulation of flow and heat transfer in a random packed bed. *Particuology*, *8*(3), 293-299.

Guo, Z., Sun, Z., Zhang, N., & Ding, M. (2019). Influence of confining wall on pressure drop and particle-to-fluid heat transfer in packed beds with small D/d ratios under high Reynolds number. *Chemical Engineering Science*, *209*, 115200.

Guo, Z., Sun, Z., Zhang, N., Ding, M., Bian, H., & Meng, Z. (2019). Computational study on fluid flow and heat transfer characteristic of hollow structured packed bed. *Powder Technology*, *344*, 463-474.

Guo, Z., Sun, Z., Zhang, N., Ding, M., & Liu, J. (2017). Pressure drop in slender packed beds with novel packing arrangement. *Powder Technology*, *321*, 286-292.

Guo, Z., Sun, Z., Zhang, N., Ding, M., & Shi, S. (2019). CFD analysis of fluid flow and particle-to-fluid heat transfer in packed bed with radial layered configuration. *Chemical Engineering Science*, *197*, 357-370.

Guo, Z., Sun, Z., Zhang, N., Ding, M., & Zhou, Y. (2019). Influence of flow guiding conduit on pressure drop and convective heat transfer in packed beds. *International Journal of Heat and Mass Transfer*, *134*, 489-502.

Halkarni, S. S., Sridharan, A., & Prabhu, S. (2016). Estimation of volumetric heat transfer coefficient in randomly packed beds of uniform sized spheres with water as working medium. *International Journal of Thermal Sciences*, *110*, 340-355.

Halkarni, S. S., Sridharan, A., & Prabhu, S. (2017). Measurement of local wall heat transfer coefficient in randomly packed beds of uniform sized spheres using infrared thermography (IR) and water as working medium. *Applied Thermal Engineering*, *126*, 358-378.

Helm, C., & Mier, M. (2019). On the efficient market diffusion of intermittent renewable energies. *Energy Economics*, *80*, 812-830.

Hu, Y., Wang, J., Yang, J., Mudawar, I., & Wang, Q. (2019). Experimental study of forced convective heat transfer in grille-particle composite packed beds. *International Journal of Heat and Mass Transfer*, *129*, 103-112.

Hu, Y., Yang, J., Wang, J., & Wang, Q. (2018). Investigation of hydrodynamic and heat transfer performances in grille-sphere composite pebble beds with DEM-CFD-Taguchi method. *Energy*, *155*, 909-920.

Ismail, K., & Henríquez, J. (2000). Solidification of PCM inside a spherical capsule. *Energy Conversion and Management*, *41*(2), 173-187.

Jia, X., Zhai, X., & Cheng, X. (2019). Thermal performance analysis and optimization of a spherical PCM capsule with pin-fins for cold storage. *Applied Thermal Engineering*, *148*, 929-938.

Karassik, I. J. (2001). *Pump handbook*.

Kenisarin, M. M., Mahkamov, K., Costa, S. C., & Makhkamova, I. (2020). Melting and solidification of PCMs inside a spherical capsule: A critical review. *Journal of Energy Storage*, *27*, 101082.

Lee, D.-Y., & Chung, B.-J. (2019). Variations of forced convection heat transfer of packed beds according to the heated sphere position and bed height. *International Communications in Heat and Mass Transfer*, *103*, 64-71.

Li, B., Zhai, X., & Cheng, X. (2019). Thermal performance analysis and optimization of multiple stage latent heat storage unit based on entransy theory. *International Journal of Heat and Mass Transfer*, *135*, 149-157.

Li, T., Xu, J., Wu, D., He, F., & Wang, R. (2019). High energy-density and power-density thermal storage prototype with hydrated salt for hot water and space heating. *Applied Energy*, *248*, 406-414.

Qian, P., Wang, J., Wu, Z., Yang, J., & Wang, Q. (2019). Performance comparison of methane steam reforming in a randomly packed bed and a grille-sphere composite packed bed. *Energy Conversion and Management*, *193*, 39-51.

Rebughini, S., Cuoci, A., & Maestri, M. (2016). Handling contact points in reactive CFD simulations of heterogeneous catalytic fixed bed reactors. *Chemical Engineering Science*, *141*, 240-249.

Romkes, S., Dautzenberg, F., Van den Bleek, C., & Calis, H. (2003). CFD modelling and experimental validation of particle-to-fluid mass and heat transfer in a packed bed at very low channel to particle diameter ratio. *Chemical Engineering Journal*, *96*(1-3), 3-13.

Sheikholeslami, M. (2018). Numerical modeling of nano enhanced PCM solidification in an enclosure with metallic fin. *Journal of Molecular Liquids*, *259*, 424-438.

Sobes, V., Forget, B., & Kadak, A. (2011). Individual pebble temperature peaking factor due to local pebble arrangement in a pebble bed reactor core. *Nuclear engineering and design*, *241*(1), 124-133.

Tian, X.-W., Xu, S.-M., Sun, Z.-H., Wang, P., Xu, L., & Zhang, Z. (2018). Experimental study on flow and heat transfer of power law fluid in structured packed porous media of particles. *Experimental Thermal and Fluid Science*, *90*, 37-47.

Toghraie, D., Afrand, M., Zadeh, A. D., & Akbari, H. A. (2018). Numerical investigation on the flow and heat transfer of a multi-lobe particle and equivalent spherical particles in a packed bed with considering the wall effects. *International Journal of Mechanical Sciences*, *138*, 350-367.

Wang, J., Guo, Q., Yang, J., Liu, Y., & Wang, Q. (2017). Experimental study of convective heat transfer in grille-sphere composite structured packed bed. *Energy Procedia*, *105*, 4782-4787.

Wang, J., Yang, J., Cheng, Z., Liu, Y., Chen, Y., & Wang, Q. (2018). Experimental and numerical study on pressure drop and heat transfer performance of grille-sphere composite structured packed bed. *Applied Energy*, *227*, 719-730.

Wang, P., Zhao, P., Xu, W., Wang, J., & Dai, Y. (2019). Performance analysis of a combined heat and compressed air energy storage system with packed bed unit and electrical heater. *Applied Thermal Engineering*, *162*, 114321.

Wang, X., Zhai, X., Wang, T., Wang, H., & Yin, Y. (2013). Performance of the capric and lauric acid mixture with additives as cold storage materials for high temperature cooling application. *Applied Thermal Engineering*, *58*(1-2), 252-260.

Yang, J., Wang, Q., Zeng, M., & Nakayama, A. (2010). Computational study of forced convective heat transfer in structured packed beds with spherical or ellipsoidal particles. *Chemical Engineering Science*, *65*(2), 726-738.

Yeboah, S., & Darkwa, J. (2019). Experimental investigations into the adsorption enhancement in packed beds using Z-Annular flow configuration. *International Journal of Thermal Sciences*, *136*, 121-134.

Zenner, A., Fiaty, K., Bellière-Baca, V., Rocha, C., Gauthier, G., & Edouard, D. (2019). Effective heat transfers in packed bed: Experimental and model investigation. *Chemical Engineering Science*, *201*, 424-436.

Zhai, X., Cheng, X., Wang, C., & Wang, R. (2015). Experimental investigation and performance analysis of a fin tube phase change cold storage unit for high temperature cooling application. *Energy and Buildings*, *89*, 9-17.

Zhang, Y., Zhang, Z., Lu, Y., Chalermsinsuwan, B., Wang, F., Zhang, H., & Wang, X. (2024). Efficient hydrate-based carbon capture system enabled by red blood cell inspired encapsulation. *Applied Energy*, *359*, 122784.

Engineering Power – *Bulletin of the Croatian Academy of Engineering* Vol. 19(3) 2024 – ISSN 1331-7210 (Print)
ISSN 2718-322X (Online)
Publisher: Croatian Academy of Engineering (HATZ), 28 Kačić Street, P.O. Box 14, HR-10000 Zagreb, Republic of Croatia
Editor-in-Chief: Prof. Vedran Mornar, Ph.D., President of the Academy
University of Zagreb, Faculty of Electrical Engineering and Computing
Editor: Prof. Bruno Zelić, Ph.D., Vice-President of the Academy
University of Zagreb, Faculty of Chemical Engineering and Technology
Guest-Editor: Prof. Neven Duić, Ph.D., University of Zagreb, Faculty of Mechanical Engineering and Naval Architecture
Activities Editor: Tanja Miškić Rogić
Editorial Board: Prof. Vedran Mornar, Ph.D., Prof. Vladimir Andročec, Ph.D., Prof. Bruno Zelić, Ph.D., Assoc. Prof. Mario Bačić, Ph.D., Prof. Neven Duić, Ph.D.
Editorial Board Address: Croatian Academy of Engineering (HATZ), "Engineering Power" – Bulletin of the Croatian Academy of Engineering, Editorial Board, 28 Kačić Street, P.O. Box 14, HR-10000 Zagreb, Republic of Croatia
E-mail: hatz@hatz.hr
Graphical and Technical Editor: Tiskara Zelina, Ltd., Zelina
Press: Tiskara Zelina, Ltd., Zelina
Circulation: 200